Distribution of scales in turbulence

Haris J. Catrakis*
Department of Mechanical and Aerospace Engineering, University of California, Irvine, California 92697
(Received 9 June 1999; revised manuscript received 3 April 2000)

The physical structure of convoluted surfaces and fluid interfaces in turbulence is quantified by a distribution of geometric scales. A scale measure suitable for multidimensional surfaces and a one-to-one correspondence between the scale distribution and the coverage dimension are used to analyze the scale dependence of the interfacial geometry. Application to concentration interfaces in a turbulent mixing flow indicates that the statistical laws exhibited at the small scales can be quantified and modeled. Based on the scale distribution, dimensionless measures of folding and wrinkling of the fluid interfaces are introduced which are useful to quantify the contributions of the large-scale and small-scale turbulent flow structure to the interfacial geometry.

PACS number(s): 47.27.Ak, 02.50.−r, 47.53.+n, 47.27.Qb

I. INTRODUCTION

In turbulence and other nonlinear complex phenomena, there is a challenge of bridging the knowledge that is beginning to be acquired with direct numerical simulations and careful experiments at low and moderate values of the nonlinearity parameter, or Reynolds number in the case of turbulence, to what needs to be known at large values of the nonlinearity parameter, or large Reynolds numbers. In the context of velocity- and vorticity-field statistics in turbulence, this question has been asked traditionally in terms of spectra or structure functions, with the Kolmogorov power-law as a good example of how one may use a power-law, in that case, to bridge length scales [1–5]. In the context of turbulent mixing, which is important practically, a crucial feature is the geometry of the fluid interfaces. How does one extrapolate knowledge of the structure of interfaces, or level sets, to high Reynolds numbers? What tools must be developed to address this issue? How should they be applied?

Turbulence-generated fluid interfaces are observed to be highly convoluted over a large range of scales, e.g., the interface(s) between two or more fluids mixed by high-Reynolds-number shear layers or jets [6,7]. For incompressible flow and mixing of a simple fluid, for example, the velocity field, $\mathbf{u}(\mathbf{x},t)$, and concentration field, $c(\mathbf{x},t)$, are governed by the Navier-Stokes and scalar evolution equations,

$$\partial_t \mathbf{u} + \mathbf{u}\cdot\boldsymbol{\nabla}\mathbf{u} = -\boldsymbol{\nabla} p + \frac{1}{\mathrm{Re}}\boldsymbol{\nabla}^2\mathbf{u}, \tag{1}$$

$$\partial_t c + \mathbf{u}\cdot\boldsymbol{\nabla} c = \frac{1}{\mathrm{Re\,Sc}}\boldsymbol{\nabla}^2 c, \tag{2}$$

in dimensionless form, constrained by mass conservation, $\boldsymbol{\nabla}\cdot\mathbf{u}=0$, and appropriate initial and boundary, or inflow and outflow, conditions. Turbulence is flow at high Reynolds numbers and, in three dimensions, is associated with nonlinear vortex stretching and near-singular behavior of the velocity gradients at large Re, resulting in complex vortical structure. If the Schmidt number is also large, i.e., for large values of the Péclet number $\mathrm{Pe}\equiv\mathrm{Re\,Sc}$, fluid interfaces may also be expected to exhibit convoluted structure, such as for the concentration isosurfaces or level sets,

$$c(\mathbf{x},t) = \mathrm{const} = c^*, \tag{3}$$

where c^* is a scalar threshold corresponding physically to a particular local degree of mixing, or composition, attained by the fluid. The resulting physical structure of the interfacial surfaces must be quantified in order to understand, predict, or compensate for a variety of phenomena that rely on molecular diffusion, chemical reactions, or electromagnetic/acoustic wave propagation across fluid interfaces, e.g., mixing, combustion, aerooptics, or aeroacoustics. The area-volume ratio of mixed-fluid interfaces, in particular, is crucial to quantify the total amount of mixing, or mixing efficiency of the flow. Classically, the statistical properties of turbulence-generated fields have been analyzed typically in Fourier space, rather than physical space, and, in particular, in terms of power spectra of derived flow measures. Descriptions based only on power spectra, however, do not retain any phase information from the Fourier transforms and, in general, cannot uniquely provide information on the physical structure of level sets or isosurfaces. Quantifying and predicting length, area, or volume properties of isosurfaces necessitates the development of a physical-space geometric framework. Beyond a minimum Reynolds number of $\mathrm{Re}\sim 10^4$, turbulent flows may be expected to be fully-developed and associated with a host of similarity properties [7]. For large values of the Péclet number, there have been proposals of geometric scaling or fractal behavior of fluid interfaces such as concentration isosurfaces or level sets. Scaling behavior of fluid interfaces would have important consequences fundamentally and practically [8–10,6,11].

In general, despite the simplicity of the governing laws, many phenomena exhibit complexity [12,13]. This can be traced to the breaking of symmetry properties of the equations by imposed initial or boundary conditions, the development of instabilities, and subsequent nonlinear pattern formation and evolution away from equilibrium leading to

*Fax: (949) 824-4028. Electronic address: catrakis@uci.edu

structures and dynamics that span a wide range of space-time scales. Far from equilibrium, the lost symmetry can be restored resulting in statistical symmetry properties which may often be understood in terms of similarity and scaling arguments. For a variety of phenomena, including turbulence, there have been suggestions and reports of power-law scaling of surfaces or interfaces [8,14,10,15]. Such conjectures and findings are cast in terms of a constant fractal dimension identified as the scaling exponent of the assumed/observed power law. Fractal geometry is able to quantify structures of a higher level of complexity than Euclidean geometry. Whereas Euclidean objects have structure on a single, large scale only, fractal objects exhibit the same structure on many different scales and are characterized by power laws [16]. A higher level of complexity yet can be expected: different structures, or structures of different complexity, may appear at different scales with more general, non-power-law statistics, e.g., lognormal, Poisson, etc. These considerations suggest a three-level hierarchy of complexity.

Level 1: complexity only at single scale—*Euclidean geometry*.

Level 2: complexity same at all scales—*power-law or fractal geometry*.

Level 3: complexity may vary with scale—*scale-dependent geometry*.

Classical examples of power-law scaling laws are isometric or proportionate scaling relations for the area, A, or volume, V, of Euclidean objects such as disks or spheres, for which $A \sim L^2$ and $V \sim L^3$ in terms of a characteristic length scale, L. Nonisometric, allometric, or disproportionate power-law scaling relations are also possible. Indeed, Galilei [17] pointed out that the bones of large animals must be scaled out of proportion to their linear dimensions in order to support the animal's weight, e.g., $R \sim L^{1.5}$, with a dimensional prefactor, where R is the bone diameter and L the length of the bone. Such fractional-power or fractal laws are linear in Richardson's log-log coverage-scale plot [18], with a negative slope given by the power-law scaling exponent or fractal dimension. Fractal geometry is a manifestation of self-similarity, both terms coined by Mandelbrot [14]. For such objects, coverage statistics are described by power laws with a constant coverage dimension, D_d, i.e.,

$$N_d(\lambda) \sim \lambda^{-D_d} \quad \text{or} \quad \frac{dN_d(\lambda)}{N_d(\lambda)} = -D_d \frac{d\lambda}{\lambda}, \tag{4}$$

where the latter form is dimensionless and $N_d(\lambda)$ is the coverage function at a scale λ in d dimensions. The coverage, $N_d(\lambda)$, counts the number of nonoverlapping boxes of size λ needed to cover the object under study, out of a λ-partition of the d-dimensional embedding space. The scale λ may refer to a temporal, spatial, or space-time scale.

In various phenomena, however, the coverage dimension, D_d, has been observed to be a smooth function of scale, i.e., $D_d(\lambda)$. In such cases, a scale-dependent coverage dimension can still be identified as a local logarithmic derivative of the coverage function,

$$D_d(\lambda) \equiv -\frac{dN_d(\lambda)/N_d(\lambda)}{d\lambda/\lambda} = -\frac{d \log N_d(\lambda)}{d \log \lambda}, \tag{5}$$

and the fractal case, i.e., $D_d(\lambda) = \text{const}$, is then a special case. If $D_d(\lambda) \neq \text{const}$, however, as may be anticipated to be the case in general, there will be no power-law-like behavior of the coverage function, i.e., $N_d(\lambda) \not\sim \lambda^{-D_d(\lambda)}$. While the coverage dimension, at a scale λ, can still be identified as the fractional decrease in coverage, $-dN_d/N_d$, per unit fractional increase in scale, $d\lambda/\lambda$, it implies the more general, nonpower law,

$$N_d(\lambda) = \exp\left\{ \int_{\lambda}^{\delta_b} D_d(\lambda') \frac{d\lambda'}{\lambda'} \right\} \tag{6}$$

[19] where δ_b is the largest scale of the object. For data of finite extent, δ_b can be computed as the size of the bounding box and $N_d(\delta_b) = 1$ by definition. The physical interpretation of the general behavior expressed in Eq. (6) is that the complexity of structures across a wide range of scales can contribute to the coverage behavior at any one λ scale.

Evidence of coverage dimensions that are smooth functions of scale has been reported, for example, for Brownian motion [19,20], coastlines [21], topographic surfaces [22], fracture-network surveys [23], lung tissue of prematurely-born rabbits [24], solar granulation [25], and the galaxy distribution in the universe [26]. Various terms have been employed to denote such non-power-law behavior: differential fractal, superfractal, semi-fractal, etc. An analytical expression for the coverage-dimension function, $D_d(\lambda)$, has also been offered for 1D Brownian motion [19] and results in a dimension that increases continuously with scale from unity, at small scales, to 2, at large scales. This expression was found to compare well with measurements of Brownian motion [20]. For the perimeter of lung tissues of prematurely-born rabbits, a coverage dimension expression which smoothly increases with scale was also proposed [24]. A suggestion of corrections to power-law scaling has also been made to describe objects that do not exhibit exact power laws in terms of exponential and logarithmic dimensions and a metadimension, in addition to the fractal dimension [27]. The three proposed dimensions appear as multiplicative corrections, however, and would result in a quantity which no longer has the meaning of a local dimension, i.e., of a local scale-logarithmic derivative of the coverage. Models of non-power-law behavior have also been proposed in terms of scale-dependent variants of fractal geometric constructions. Examples are scale-dependent Cantor dust [23] and scale-dependent Koch islands [21]. The analysis of such models has been conducted on a case-by-case basis.

A framework will be described and demonstrated below which can quantify the scale dependence of the geometry of convoluted surfaces and interfaces [28,29]. The proposed framework establishes a fundamental, one-to-one correspondence between coverage statistics and the underlying distribution of scales, in the form of a transform pair, and can be used to quantify multidimensional geometries. There are other means to analyze multiscale phenomena, e.g., in terms of multifractals or wavelets. Of particular interest here is the development of a framework based on a particular measure of scale that will permit a direct connection to coverage statistics of fluid interfaces and hence space-filling properties such as the area-volume ratio. In addition to the practical interest in such quantities in the context of mixing, there is a

fundamental interest concerned with the small-scale geometry of the fluid interfaces and the possible development of singularities, or near-singularities, in the vorticity field of unsteady spatially-three-dimensional high-Reynolds-number flows, associated with local growth of the velocity by nonlinear vortex stretching. Such questions are important physically because they may shed light on the nature of regions of high dissipation of energy and large rate of molecular mixing, and because they may lead to developments of canonical or universal models of small-scale structure [30].

II. DISTRIBUTION OF SCALES

There are numerous observations of phenomena whose structure and dynamics span a wide range of space-time scales [14,13]. How are such scales distributed? What is a useful measure of scale for this purpose? In the context of fluid interfaces generated by high-Reynolds-number turbulent flows, such as concentration interfaces, density isosurfaces, or vortical interfaces, the surfaces are unsteady and three-dimensional spatially, in general. It appears that fluid interfaces can be highly convoluted over a wide range of scales but may also exhibit simple, organized, large-scale features directly deducible from the large structures [31–35]. A quantitative description of the interfacial geometry is needed, ideally one that would aid in discerning the contributions of the large-scale and small-scale turbulent flow structure to the geometric features of the interface. The framework described below offers a means to quantify the distribution, or probability density function (PDF), of scales for convoluted surfaces such as fluid interfaces in turbulence. A quantitative measure of scale is necessary for this purpose. While there are different ways to quantify scales and their distributions, we would like to make a connection to coverage statistics and dimensions, and, thereby, to extend fractal geometry and quantify the scale-dependence of length, area, or volume measures. In 1D space, we will be concerned, for example, with level sets consisting of points that can arise as crossings of a certain threshold of a 1D physical signal in space or time. These crossings, in turn, may be viewed as linear transects of corresponding surfaces or interfaces in higher-dimensional space. The notion of coverage dimension remains useful in scale-dependent geometries as it provides a quantitative measure of the geometric complexity at a given scale.

Allowing for a coverage dimension that may vary continuously with scale, we proceed to investigate the consequences of a scale-dependent coverage-dimension function, $D_d(\lambda)$. We will consider the coverage of a level set, although the concepts apply to other geometric objects. In practice, coverage statistics of a level set are computed by a partitioning/box-counting algorithm: a δ_b-sized bounding box containing the level set is first partitioned into $N_{d,\mathrm{tot}(\lambda)}$ nonoverlapping, contiguous λ-sized tiles in 1D, squares or rectangles in 2D, cubes or parallelepipeds in 3D, etc., and then the number $N_d(\lambda)$ of such λ elements that cover the level set is counted. By definition, $0 \leqslant N_d(\lambda) \leqslant N_{d,\mathrm{tot}(\lambda)}$. This naturally leads to the dimensionless coverage fraction,

$$F_d(\lambda) \equiv \frac{N_d(\lambda)}{N_{d,\mathrm{tot}(\lambda)}} = \left(\frac{\lambda}{\delta_b}\right)^d N_d(\lambda) = \exp\left\{ -\int_\lambda^{\delta_b} [d - D_d(\lambda')] \frac{d\lambda'}{\lambda'} \right\} \tag{7}$$

[36], such that $0 \leqslant F_d(\lambda) \leqslant 1$ with $F_d(\delta_b) = 1$. The coverage fraction measures the degree to which the object fills space. We can consider the case $\delta_b = \infty$ without loss of generality. The proviso ''interior to the bounding box'' will be implied for the finite-δ_b case. The ensemble-averaged coverage fraction, denoted in the following also as $F_d(\lambda)$, can be identified as the geometric probability that a randomly-placed λ box, interior to the bounding box, contains part of the set, i.e.,

$$F_d(\lambda) = p_c(\lambda) = 1 - p_e(\lambda), \tag{8}$$

where $p_c(\lambda)$ is the probability that a randomly-placed λ box contains at least some part of the level set, and $p_e(\lambda)$ is the probability that a randomly-placed λ-box does not contain any part of the level set. With this interpretation of the coverage fraction as a geometric probability, the connection between coverage statistics and scale distributions can be made.

In one-dimensional space, the coverage dimension of level sets consisting of points can be connected to the probability density function (PDF) of the ''gaps'' between the successive points, i.e., the point spacing. An example of a point set is the set of level crossings of a particular threshold in a scalar or velocity-component signal in a turbulent flow. Consider a stochastic, statistically-homogeneous, point process, in space or time, with a distribution of spacing scales, i.e., interval-lengths between successive events of the process, described by a PDF, $p_1(l)$, where $l \geqslant 0$ denotes a spacing scale. From dimensional and geometric considerations, the fraction of length spanned by an l scale will be $m_1(l) \propto l\, p_1(l)$. This can be viewed also as the geometric weighting of the scales. The probability density that a random location, with uniform measure on the real line, lies in an l spacing can be written, therefore, as

$$m_1(l) = \frac{l\, p_1(l)}{l_m}, \qquad \text{where} \quad l_m \equiv \int_0^\infty l\, p_1(l)\, dl, \tag{9}$$

and l_m can be interpreted as the mean spacing scale. The geometric probability that a λ tile, randomly located on the real line with uniform measure, is ''empty,'' i.e., contains no points, can be written as

$$\begin{aligned} p_e(\lambda) &= \int_0^\infty g_e(\lambda|l)\, m_1(l)\, dl \\ &= \int_\lambda^\infty \left(1 - \frac{\lambda}{l}\right) m_1(l)\, dl \\ &= \int_\lambda^\infty \left(\frac{l-\lambda}{l_m}\right) p_1(l)\, dl, \end{aligned} \tag{10}$$

where $g_e(\lambda|l)$ is the conditional probability that a randomly-placed λ tile contains no transitions, given that it lies in an l spacing; cf. Fig. 1. The probability that a λ tile lies in an l spacing is given by the geometric weighting of the scales, $m_1(l)$, cf. Eq. (9). By a λ tile lying in an l spacing we mean that a reference point of the tile, e.g., the left end point of the tile, lies in an l spacing. The coverage fraction can be expressed in terms of the spacing-scale PDF, as

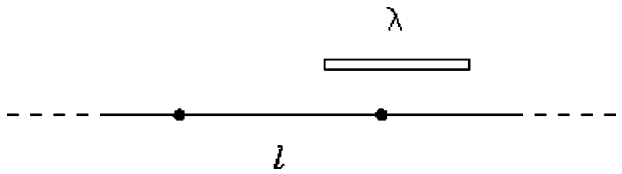

FIG. 1. Schematic of interfacial crossings along a linear transect indicating a spacing scale, l, and a coverage scale, λ.

$$F_1(\lambda)=\frac{1}{l_m}\int_0^{\lambda}\int_{\lambda'}^{\infty}p_1(l)dl\,d\lambda', \tag{11}$$

which can be interpreted geometrically as the fraction of length spanned by spacing scales with $l<\lambda$ and a contribution from spacing scales with $l>\lambda$. The limiting behavior of the coverage fraction, at small scales, is, $F_1(\lambda)\sim\lambda/l_m\rightarrow 0$, as $\lambda\rightarrow 0$, i.e., the mean spacing scale, l_m, alone, determines the small-λ scaling. At the large scales or $\lambda\rightarrow\infty$, $F_1(\lambda)\rightarrow 1$, as expected. The coverage dimension, cf. Eq. (5), can be expressed too in terms of the PDF of spacing scales,

$$D_1(\lambda)=1-\frac{\lambda\int_{\lambda}^{\infty}p_1(l)dl}{\int_0^{\lambda}\int_{\lambda'}^{\infty}p_1(l)dl\,d\lambda'}, \tag{12}$$

which may be interpreted in terms of the fraction of length spanned by the spacing scales. This implies that the small-scale and large-scale limiting behavior of the coverage dimension will be, respectively, $D_1(\lambda\rightarrow 0)\rightarrow 0$ and $D_1(\lambda\rightarrow\infty)\rightarrow 1$, as required for the coverage of 1D point sets. The relation expressed in Eq. (12) can be viewed as a forward scale-distributions transform, connecting $p_1(l)$ to $D_1(\lambda)$. It can be used, therefore, to transform scale distributions into their corresponding coverage dimensions. The inverse scale-distributions transform, connecting the coverage-dimension function to its corresponding PDF of spacing scales can also be obtained,

$$p_1(l)=\frac{l_m}{l^2}\left\{D_1(l)[1-D_1(l)]+l\frac{dD_1(l)}{dl}\right\}\times\exp\left\{-\int_l^{\infty}[1-D_1(l')]\frac{dl'}{l'}\right\}, \tag{13}$$

where the mean scale, l_m, can be expressed as

$$l_m=\lim_{l\rightarrow 0}\left\{l\exp\left[\int_l^{\infty}[1-D_1(l')]\frac{dl'}{l'}\right]\right\}. \tag{14}$$

An equivalent relation was obtained, by a different derivation, for zero crossings of stochastic Gaussian functions [37]. Extensive related results and properties have been derived before for the special case of Poisson statistics [38,39], but the present treatment is neither restricted to nor relies on the notion of Poisson behavior. The relations expressed in Eqs. (12) and (13) constitute the general 1D scale-distribution transform pair. An alternative measure of geometric scale, in 1D, that can also be connected to coverage statistics, is the *largest-empty-tile* (LET) scale. This scale measure will prove useful in extending the scale-distributions framework to higher dimensions, further below. The LET scale is defined as the size of the largest tile, centered at a random location, that is ''empty,'' i.e., does not contain any part or point of the set. It can be viewed as a first-waiting time scale, in the context of temporal point processes. The PDF of this scale, $f_1(\lambda)$, can also be interpreted as the probability (density) that a random point is a distance $\lambda/2$ away from the nearest element of the point set. Equivalently, $f_1(\lambda)$ is proportional to the number fraction of intervals of size greater than λ. If $p_1(l)$ is finite, i.e., if the spacing-scale distribution exhibits no singularities, then it can be shown that

$$f_1(\lambda)=\frac{1}{l_m}\int_{\lambda}^{\infty}p_1(l)dl=\frac{dF_1(\lambda)}{d\lambda}, \tag{15}$$

which is relevant to bounded, continuous distributions such as lognormal, power-law, Poisson, etc. These considerations result in the LET-scale distribution transform pair,

$$D_1(\lambda)=1-\frac{\lambda f_1(\lambda)}{\int_0^{\lambda}f_1(\lambda')d\lambda'} \tag{16}$$

and

$$f_1(\lambda)=\frac{1-D_1(\lambda)}{\lambda}\exp\left\{-\int_{\lambda}^{\infty}[1-D_1(\lambda')]\frac{d\lambda'}{\lambda'}\right\}. \tag{17}$$

In the 1D framework, the spacing scale, e.g., distance between successive level crossings, is a useful scale measure which can be connected to coverage statistics. In d-dimensional space, however, the spacing scale does not generalize naturally. A different scale measure is needed, therefore. The significance of the LET scale is that it can be generalized naturally to higher dimensions.

In d-dimensional space, the coverage fraction, $F_d(\boldsymbol{\lambda})$, will in general be a function of the scale vector, $\boldsymbol{\lambda}\equiv(\lambda_1,\lambda_2,\ldots,\lambda_d)$. For example, for 4D space-time data, $\boldsymbol{\lambda}=(\lambda_x,\lambda_y,\lambda_z,\lambda_t)$. Under certain symmetry conditions, indicated by the physical nature of the problem, it will be useful to consider the dependence of the coverage fraction on the scalar scale, λ, defined as a geometric mean, $\lambda=(\lambda_1\lambda_2\ldots\lambda_d)^{1/d}$. For the case of round turbulent jets, for example, slices of the concentration field normal to the jet axis will be statistically axisymmetric so that it will be useful to choose $\lambda=(\lambda_x\lambda_y)^{1/2}$, where the λ_x and λ_y scales in the box-counting and partitioning process are pegged to the bounding-box scales, δ_x and δ_y. The coverage fraction, $F_d(\lambda)$, can be identified as the geometric probability that a randomly-placed λ box covers part of $\mathcal{S}$, where $\mathcal{S}$ denotes the set under study, as noted in the discussion of Eq. (8), The set $\mathcal{S}$ could consist of points, lines, surfaces, etc., embedded in the d-dimensional space. The coverage fraction can be interpreted as a cumulative distribution function of a particular measure of scale. The differential coverage fraction can be associated with a PDF, $f_d(\lambda)$, where

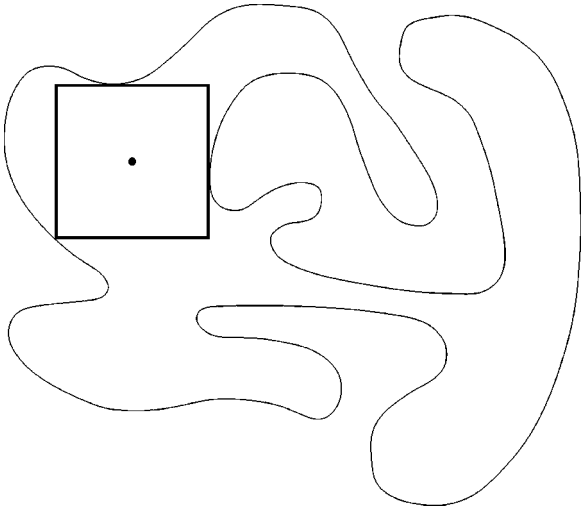

FIG. 2. Schematic of a fluid interface and a largest empty box (LEB) of size λ. The LEB scales are the sizes of the largest possible boxes, centered at random locations, that do not contain any part of the interface.

$$f_d(\lambda) \equiv \frac{dF_d(\lambda)}{d\lambda}. \tag{18}$$

The PDF, $f_d(\lambda)$, can be interpreted geometrically as the PDF of a particular measure of scale: the *largest-empty-box* (LEB) scale, λ, defined as the size of the largest box randomly placed, that is empty, i.e., covers no part of $\mathcal{S}$ (see Fig. 2). Equivalently, the LEB scale λ is a measure of (twice) the distance from a point P to the nearest element of $\mathcal{S}$. The LEB-scale distribution (PDF), $f_d(\lambda)$, satisfies the required normalization condition over the range of spatial scales, i.e., $\int_0^\infty f_d(\lambda)d\lambda = F_d(\infty) - F_d(0) = 1$. The coverage dimension, $D_d(\lambda)$, can be expressed, therefore, in terms of the distribution of LEB scales, $f_d(\lambda)$, i.e.,

$$D_d(\lambda) = d - \frac{\lambda f_d(\lambda)}{\int_0^\lambda f_d(\lambda')d\lambda'}, \tag{19}$$

which is invertible and yields the LEB-scale PDF from the coverage dimension, $D_d(\lambda)$, directly, i.e.,

$$f_d(\lambda) = \frac{d - D_d(\lambda)}{\lambda} \exp\left\{ -\int_\lambda^\infty [d - D_d(\lambda')]\frac{d\lambda'}{\lambda'} \right\}. \tag{20}$$

These relations constitute the d-dimensional scale-distribution transform pair. The above framework is not restricted to statistically homogeneous geometries. In general, the probability of covering the set with a λ box, interior to the δ_b box, will be a function of position within the δ_b box. For a set contained in a d-dimensional bounding box of size δ_b, the coverage fraction, $F_d(\lambda)$, can be identified as the geometric probability that a randomly-placed λ box, interior to the outer δ_b box, covers part of $\mathcal{S}$. For spatially inhomogeneous statistics, the function $F_d(\lambda)$ represents the probability of coverage for a λ tile placed in the δ_b box without regard to its location.

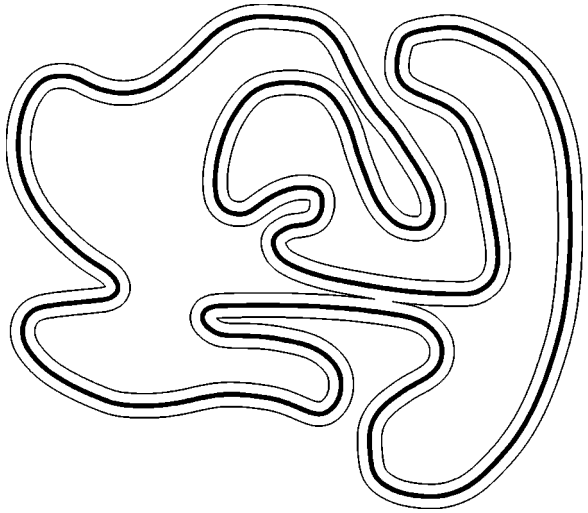

FIG. 3. Schematic of surfaces constructed such that they are equidistant to the fluid interface. The offset distance is $\lambda/2$, where λ is the LEB scale corresponding to LEBs centered on these surfaces.

An additional useful interpretation of the LEB-scale PDF, $f_d(\lambda)$, can be made as a measure of area/volume properties. From the definition of a LEB scale, we can expect that the set of points at which the size of the LEB scale is λ will have a measure associated to them (length, area, etc.) determined by $f_d(\lambda)$. This set of points will be at a constant distance, $\lambda/2$, away from the level set. For example, for the coverage of a level-set contour in 2D or isosurface in 3D, this set of points would be curves or surfaces, respectively, equidistant to the level set and spaced by a distance given by $\lambda/2$. This is illustrated in Fig. 3 which shows that, in general, there will be a family of surfaces on either side of the level set. We can expect, *a priori*, that the LEB-scale PDF will be, in general, an increasing function of decreasing λ. The LEB-scale PDF, $f_d(\lambda)$, can be interpreted as a scale-dependent measure of the surface-area/volume ratio, in 3D, of LEB surfaces that are equidistant from the isosurface by a distance $\sim\lambda/2$. In particular, the small-scale limit of the LEB-scale PDF, i.e.,

$$\lim_{\lambda \to 0} f_d(\lambda) = \frac{1}{\lambda_m}, \tag{21}$$

where the scale λ_m is the mean LEB scale, is a measure of the area-volume ratio, A_d/V_d, where A_d is the surface area of the level set and V_d is a normalizing volume, e.g., the volume spanned by the embedding space. The area-volume ratio itself offers another (inverse) length scale,

$$\frac{A_d}{V_d} = \frac{1}{\lambda_\sigma}. \tag{22}$$

While for the special case of Poisson statistics this inverse area-volume ratio scale is identical to the mean LEB scale, i.e., $\lambda_\sigma = \lambda_m$, we can expect that in general, $\lambda_\sigma \neq \lambda_m$, as is the case in turbulence.

To quantify the structure of multidimensional surfaces in general, it will be necessary to analyze the dependence of coverage statistics on all scales and the corresponding distribution of such scales, in terms of the scale vector, $\boldsymbol{\lambda} \equiv (\lambda_1, \lambda_2, \ldots, \lambda_d)$. The coverage fraction, $F_d(\boldsymbol{\lambda})$, corresponding to the coverage, $N_d(\boldsymbol{\lambda})$, is

$$F_d(\boldsymbol{\lambda}) = \frac{N_d(\boldsymbol{\lambda})}{\prod_{i=1}^{d} \left(\frac{\delta_i}{\lambda_i}\right)}, \tag{23}$$

cf. Eq. (7), where $\boldsymbol{\delta} = (\delta_1, \delta_2, \ldots, \delta_d)$ is the scale vector corresponding to the multidimensional bounding box. The coverage and coverage fraction are related to the coverage dimension, $\mathbf{D}_d(\boldsymbol{\lambda})$, by

$$\mathbf{D}_d(\boldsymbol{\lambda}) \equiv -\frac{\partial \log N_d(\boldsymbol{\lambda})}{\partial \log \boldsymbol{\lambda}} \equiv \mathbf{I} - \frac{\partial \log F_d(\boldsymbol{\lambda})}{\partial \log \boldsymbol{\lambda}}, \tag{24}$$

i.e., the coverage dimension becomes a vector, $\mathbf{D}_d \equiv (D_d^{(1)}, D_d^{(2)}, \ldots, D_d^{(d)})$, where $\mathbf{I}$ here denotes the unity vector $\mathbf{I} \equiv (1,1,\ldots,1)$. In the particular case of fractal or self-affine scaling, i.e., if $\mathbf{D}_d(\boldsymbol{\lambda})$ is a constant or $\boldsymbol{\lambda}$-independent vector, $N_d(\boldsymbol{\lambda}) \sim \lambda_1^{D_d^{(1)}} \lambda_2^{D_d^{(2)}} \ldots \lambda_d^{D_d^{(d)}}$, cf. discussion of the power law in Eq. (4). In the general case,

$$N_d(\boldsymbol{\lambda}) = \exp\left(\sum_{i=1}^{d} \int_{\lambda_i}^{\delta_i} D_d^{(i)}(\lambda_i) \frac{d\lambda_i}{\lambda_i} \right), \tag{25}$$

so that, as required at the largest scales, $N_d(\boldsymbol{\delta}) = 1$. In the scale-dependent case, in other words, the complexity of structures at different scales can contribute to the coverage behavior at a particular scale. The LEB-scale distribution becomes a joint probability density function of LEB scales, $f_d(\boldsymbol{\lambda})$, normalized so that

$$\int_0^{\delta_1} \ldots \int_0^{\delta_d} f_d(\boldsymbol{\lambda}) d\boldsymbol{\lambda} = 1, \tag{26}$$

for data bounded in a multdimensional $\boldsymbol{\delta}$-sized bounding box. This scalar-valued PDF retains the original geometric meaning, i.e., as the probability density of finding a $\boldsymbol{\lambda}$-sized largest empty box (LEB), but is now a joint probability density of the LEB-scale vector, $\boldsymbol{\lambda}$.

These considerations are particularly useful for quantifying and modeling the spatial or space-time structure of convoluted surfaces. For example, this framework is useful in the context of quantifying the physical structure of fluid interfaces and the total amount of mixing or mixing efficiency in turbulent flows. The space-time analysis enabled by this framework is relevant to the study of the evolution of surfaces in general, and of the dynamics and velocity distribution of spatial structures of different sizes and shapes in turbulence, in particular, such as mixed-fluid interfaces and vortical structures.

III. STRUCTURE OF CONVOLUTED SURFACES AND FLUID INTERFACES

In the context of turbulent flows, Poisson and lognormal scale distributions are particularly relevant as they have been reported for level crossings of velocity and scalar signals measured in various flows [40,41]. In grid turbulence, exploratory investigations of zero crossings of 1D velocity signals in grid turbulence [42] measured the mean spacing scale, l_m, which determines the small-scale behavior of the coverage fraction, $F_1(\lambda \to 0) \sim \lambda / l_m$. In turbulent boundary layers, measurements of the spacing PDF were reported to exhibit Poisson statistics [40]. For Poisson random point processes, in general, i.e.,

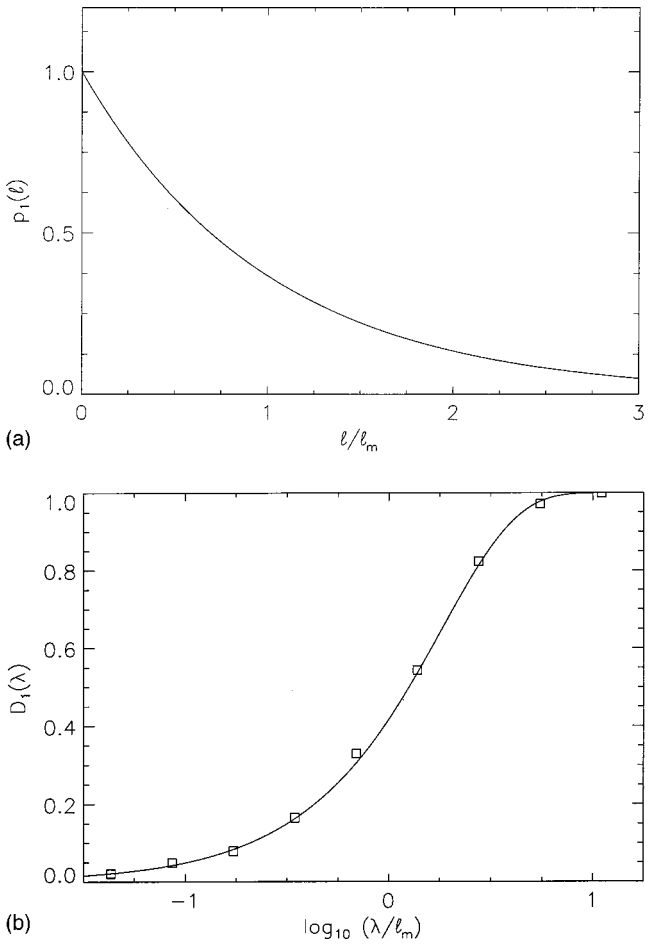

FIG. 4. Scale distribution (a) and dimension as a function of scale (b) for Poisson point processes. Theory: solid line; simulations: squares.

$$p_1(l)dl = \exp(-l/l_m) dl/l_m, \tag{27}$$

the coverage dimension function is

$$D_1(\lambda) = 1 - \frac{\lambda/l_m}{e^{\lambda/l_m} - 1}. \tag{28}$$

Figure 4 compares $D_1(\lambda)$ to an ensemble-averaged result from five Monte-Carlo simulations. For each simulation, a randomly-placed L-record, where $L/l_m = 1000$, was partitioned successively into smaller λ intervals and the coverage fraction computed for each λ. The standard deviation of the ensemble-averaged Monte Carlo estimates is smaller than the symbol size. Poisson processes, in general, therefore, are associated with a coverage dimension that increases smoothly with scale. This was pointed out, qualitatively, in early studies of the fractal facets of turbulence [9]. Lognormal statistics for the PDF of spacings derived from 1D level crossings have also been reported. Examples include scalar measurements in turbulent jets [43,29] or in plumes dispersing in the

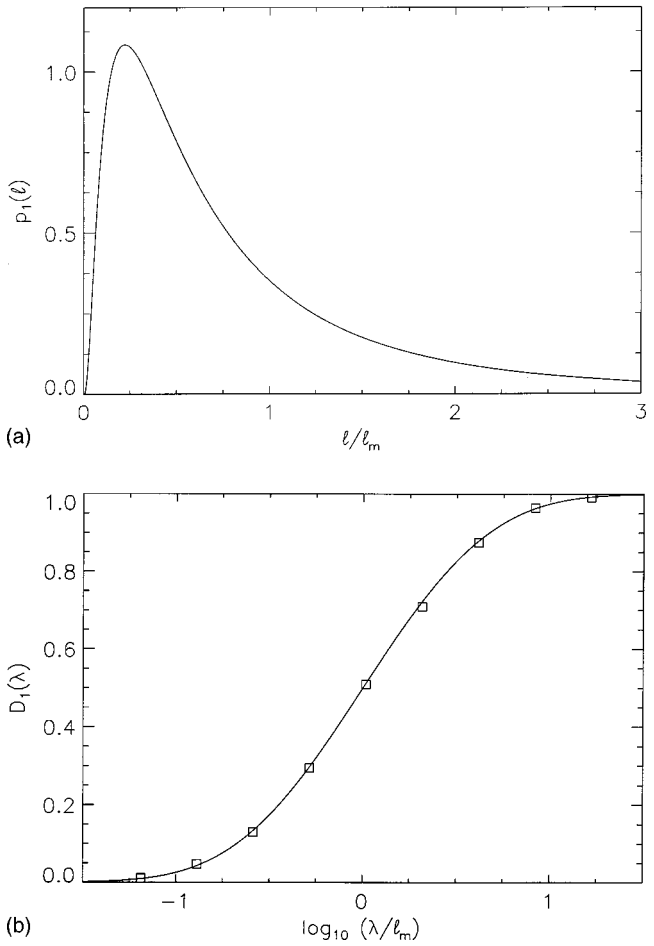

FIG. 5. Scale distribution (a) and dimension as a function of scale (b) for lognormal point statistics. Theory: solid line; simulations: squares.

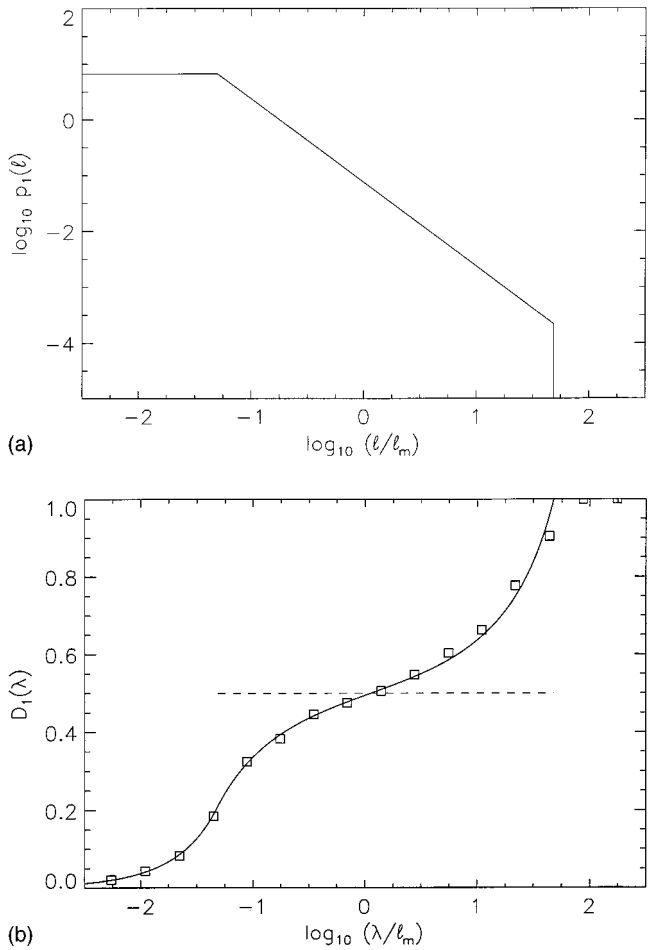

FIG. 6. Scale distribution (a) and dimension as a function of scale (b) for 1D power-law statistics over three decades ($\nu = 3/2, l_2/l_1 = 10^3$). Theory: solid line; simulations: squares.

atmospheric surface layer [41], and velocity measurements in turbulent boundary layers [40]. For a lognormal spacing-scale PDF, i.e.,

$$p_1(l)dl = \exp\{-[\ln(l/l_m)/\sigma + \sigma/2]^2/2\}dl/(\sqrt{2\pi}\sigma l), \tag{29}$$

the coverage dimension is

$$D_1(\lambda) = 1 - \left\{1 + \frac{l_m}{\lambda}\left[\frac{1+\mathrm{erf}[(\ln(\lambda/l_m)/\sigma - \sigma/2)/\sqrt{2}]}{1-\mathrm{erf}[(\ln(\lambda/l_m)/\sigma + \sigma/2)/\sqrt{2}]}\right]\right\}^{-1}. \tag{30}$$

This is compared with ensemble-averaged results from five Monte-Carlo simulations with $L/l_m = 3000$ in Fig. 5. Similar qualitative behavior was also observed through other simulations based on a lognormal PDF [43]. Comparison of Figs. 4 and 5 shows that Poisson and lognormal statistics are associated with a coverage dimension function that exhibits similar ''S-shaped'' behavior. In both cases, therefore, the dimension increases smoothly with scale with a scale dependence that reflects the underlying spacing-scale distribution. There are two notable differences. The lognormal dimension exhibits a reflection symmetry in $\log\lambda$ coordinates about the mean-scale point [$\lambda = l_m$, $D_1(\lambda) = 1/2$]. Second, the additional degree of freedom afforded by lognormal statistics in terms of the standard-deviation parameter, σ, allows the spread in the variation of $D_1(\lambda)$ values with scale to be varied. It is interesting that the qualitative difference in $p_1(l)$ for small spacing scales, in the lognormal and Poisson cases, does not have a significant effect in the coverage behavior, cf. Figs. 4 and 5. This can also be seen from Eq. (12). Power-law statistics for $p_1(l)$, over a finite range of scales, e.g.,

$$p_1(l)dl = \begin{cases} a\,dl/l_1, & \text{for } l < l_1, \\ a(l/l_1)^{-\nu}dl/l_1, & \text{for } l_1 < l < l_2, \\ 0 & \text{for } l_2 < l, \end{cases} \tag{31}$$

correspond to a dimension function,

$$D_1(\lambda) = \begin{cases} \dfrac{\lambda/l_1}{2(\nu - \alpha^{1-\nu})/(\nu-1) - \lambda/l_1}, & \text{for } l < l_1, \\ \dfrac{\beta l_1/\lambda + (1-\nu)(l_2/\lambda)^{\nu-1}}{2 - \nu + \beta l_1/\lambda - (l_2/\lambda)^{\nu-1}}, & \text{for } l_1 < l < l_2, \\ 1, & \text{for } l_2 < l, \end{cases} \tag{32}$$

where $a = 1 - 1/\nu$, $\alpha \equiv l_2/l_1$, $\beta \equiv \nu(\nu-1)\alpha^{\nu-1}/2$, and $l_m = (\nu-1)(\alpha^{2-\nu} - \nu/2)/[(2-\nu)/(\nu - \alpha^{1-\nu})]$. This is plotted in Fig. 6, for $\nu = 3/2$ and $l_2/l_1 = 1000$, i.e., for power-law

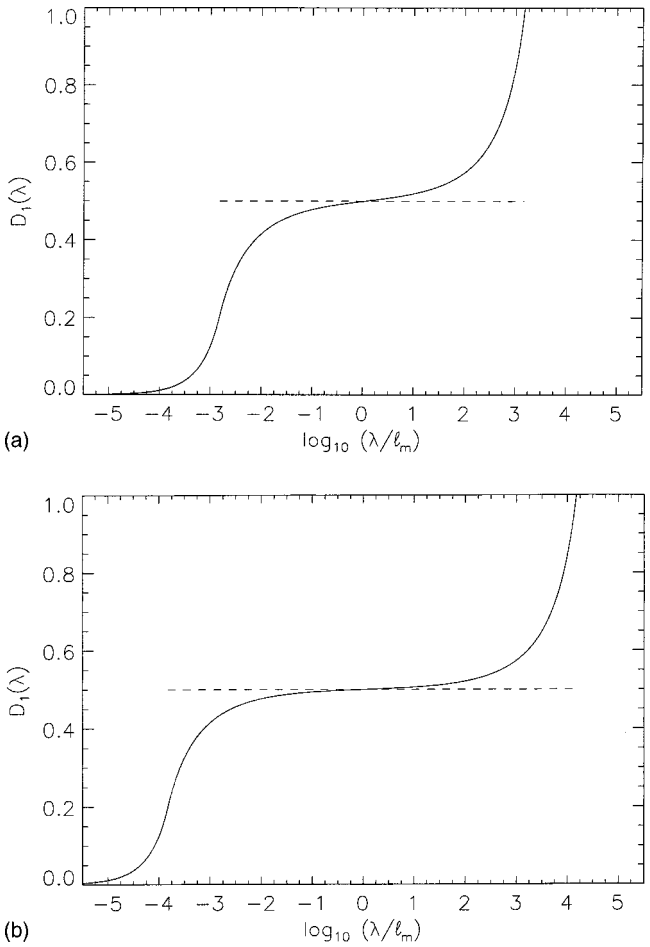

FIG. 7. Coverage dimension as a function of scale for power-law point statistics imposed over six decades (a) and over eight decades (b), with $\nu=3/2$.

scaling imposed over three decades. Comparison to five Monte Carlo simulations with $L/l_m=4000$ is also shown. The limiting case, $l_2/l_1 \gg 1$, for a power-law distribution of scales is interesting since it may be expected to correspond to a vanishing finite-size effect. It can be shown, from Eq. (12), that

$$D_1(\lambda) \rightarrow \text{const} = \nu - 1 \quad \text{for} \quad l_1 \ll l \ll l_2, \tag{33}$$

for $1<\nu<2$, i.e., the coverage dimension is expected to asymptote to a scale-independent plateau in this limit. This is examined in Fig. 6 where the dashed line corresponds to the case of $\nu=3/2$, for example. It is surprising that the coverage dimension does not display a clear plateau, even though the imposed power-law scaling spans, in this case, three decades of spacing scales. It follows, therefore, that the finite range of scaling has a strong influence on the coverage-dimension behavior. This observation is significant because it implies that finite-range power-law scaling of the scale distribution will not translate to a clear plateau in $D_1(\lambda)$ unless the scaling range is very large. For example, Fig. 7 shows the corresponding results for power-law scaling imposed over eight or ten decades. Again, it is surprising how slowly the coverage-dimension behavior approaches a plateau as the number of decades of imposed scaling is increased. If, on the other hand,

$$D_1(\lambda) = D_1 = \text{const}, \tag{34}$$

or, equivalently, $F_1(\lambda) \sim \lambda^{1-D_1}$, for $\lambda_1 \ll \lambda \ll \lambda_2$, then Eq. (13) can be used to show that

$$p_1(l) \sim l^{-D_1-1}, \tag{35}$$

with a dimensional prefactor. Therefore, while a power-law coverage fraction, over a range of scales, implies a power-law $p_1(l)$ in the same range, the converse is not true. This is a manifestation of the non-local, integral nature of the forward transform, cf. Eq. (12) and related discussion. A special case of the continuous, power-law scale PDF of Eq. (31), for a power-law exponent of $\nu=1$, has a coverage dimension which increases continuously with scale, as shown in Fig. 8 (left). Another special case of Eq. (31) is a power-law PDF with an exponent of $\nu=2$ and this has a coverage dimension which also increases smoothly with scale, as shown in Fig. 8 (right). The case $\nu=1$ is significant because it involves a simple, dimensionless weighting of scales which has been used in the description of turbulent shear-layer mixing [44]. The coverage dimension function need not be monotonic. For a single-scale PDF, e.g., equally-spaced points on a line, the coverage dimension can be shown to exhibit a step-increase at the characteristic scale of the PDF. This behavior implies that the only change in the complexity of the set, as a function of scale, occurs at the single characteristic scale of the PDF, as may be argued *a priori*. A two-scale PDF,

$$p_1(l) = \frac{1}{2}\delta(l-l_1) + \frac{1}{2}\delta(l-l_2), \tag{36}$$

has the coverage dimension

$$D_1(\lambda) = \begin{cases} 0, & \lambda < l_1, \\ \dfrac{1}{1+\lambda/l_1}, & l_1 < \lambda < l_2, \\ 1, & l_2 < \lambda, \end{cases} \tag{37}$$

as shown in Fig. 9 (left). The analytical coverage dimension changes only in the range of scales bounded by the two characteristic scales, and decreases with increasing scale, in that range, so that the behavior of the coverage dimension is non-monotonic. This behavior is confirmed by numerical results from 4 Monte Carlo simulations with $L/l_m=3000$, also shown in Fig. 9 (left). The discrepancy, at one of the smaller scales, between analysis and simulation stems from the discrete nature of scales employed in the box counting. Discrete fractal-like objects can also be generated, corresponding to stochastic statistically-homogeneous variants of well-known fractal sets,

$$p_1(l) = \frac{a-1}{a^N-1}\sum_{k=0}^{N-1} a^k \delta\left(l - \frac{l_0}{b^k}\right), \tag{38}$$

with a coverage dimension function,

$$D_1(\lambda)=\begin{cases} 0, & \lambda<\dfrac{l_0}{b^{N-1}}, \\ \dfrac{\sum_{i=k+1}^{N-1}\left(\dfrac{a}{b}\right)^i}{\sum_{i=k+1}^{N-1}\left(\dfrac{a}{b}\right)^i+\dfrac{\lambda}{l_0}\sum_{i=0}^{k}a^i}, & \begin{cases}\dfrac{l_0}{b^{k+1}}<\lambda<\dfrac{l_0}{b^k}, \\ k=0,\ldots,N-1,\end{cases} \\ 1, & l_0<\lambda. \end{cases} \tag{39}$$

Such objects have discrete-scale PDFs as opposed to the continuous-scale PDFs studied above. This scale PDF is nonzero at scales generated by a power-law with a single characteristic scale l_0 and parameter b. The probability densities are delta functions at these scales, generated from another power-law with parameter a. The parameters a and b, and the scale l_0, can be chosen to study several stochastic variations of the Cantor set. As an example, $a=2$ and $b=3$ would correspond to the stochastic version of the classical fractal middle-third Cantor set. Ten generations of this set result in a coverage dimension shown in Fig. 9 (right). Multiple regions of nonmonotonicity are evident. The coverage dimension seems to develop a plateau with superimposed oscillations, at a value near the $D_1=\log 2/\log 3\simeq 0.63$ for the inhomogeneous Cantor set in the small-scale limit, and is indicated as a dashed line.

An example of a concentration field, $c(x,y)$, measured in a liquid-phase turbulent jet is depicted in Fig. 10. The image is a two-dimensional spatial slice recorded at a far-field location of $z/d_0\simeq 275$ nozzle-exit diameters and in the similarity plane, i.e., normal to the jet axis, employing laser-induced

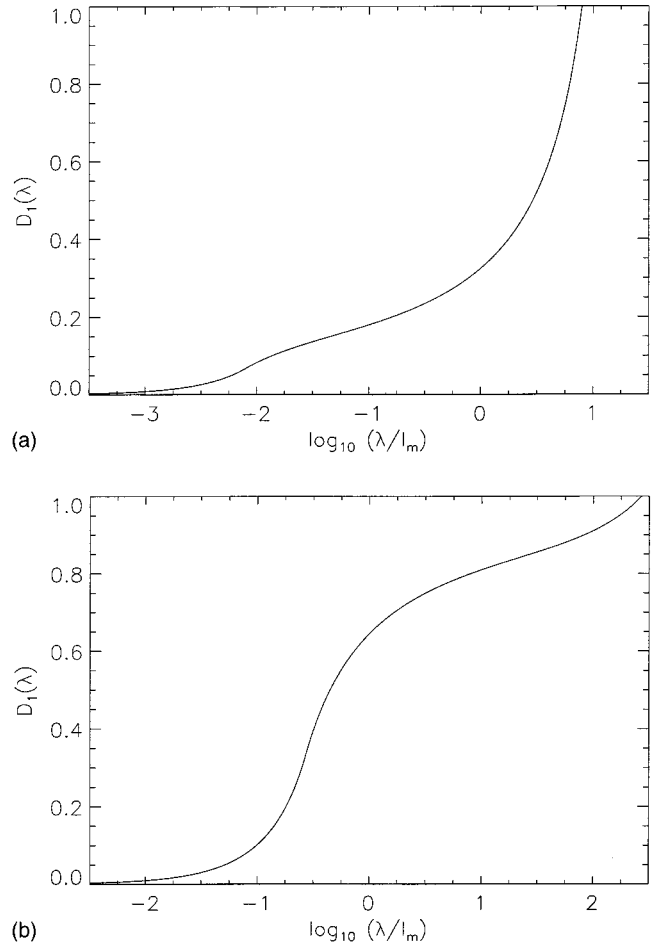

FIG. 8. (a) Coverage dimension for a continuous power-law PDF of spacing scales with $\nu=1$, cf. table entry 1.7. (b) Coverage dimension, $D_1(\lambda)$, for a continuous power-law PDF of spacing scales with $\nu=2$, cf. table entry 1.8.

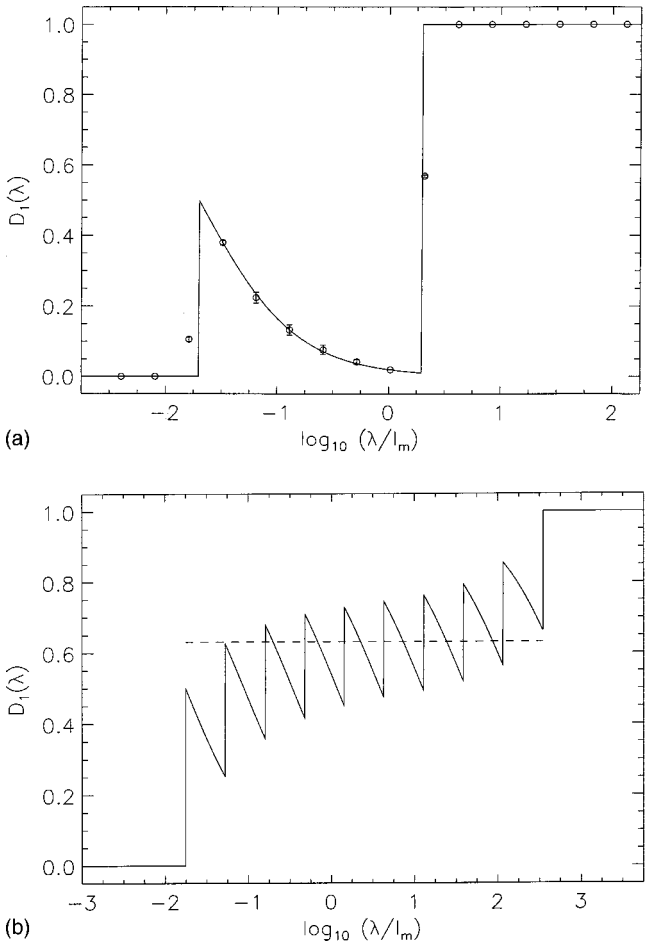

FIG. 9. (a) Coverage dimension for two-scale PDF, and results from four Monte Carlo simulations with $L/l_m=3000$. (b) Coverage dimension for a discrete power-law PDF with $a=2$ and $b=3$, corresponding to a stochastic version of the classical fractal Cantor set, for ten generations.

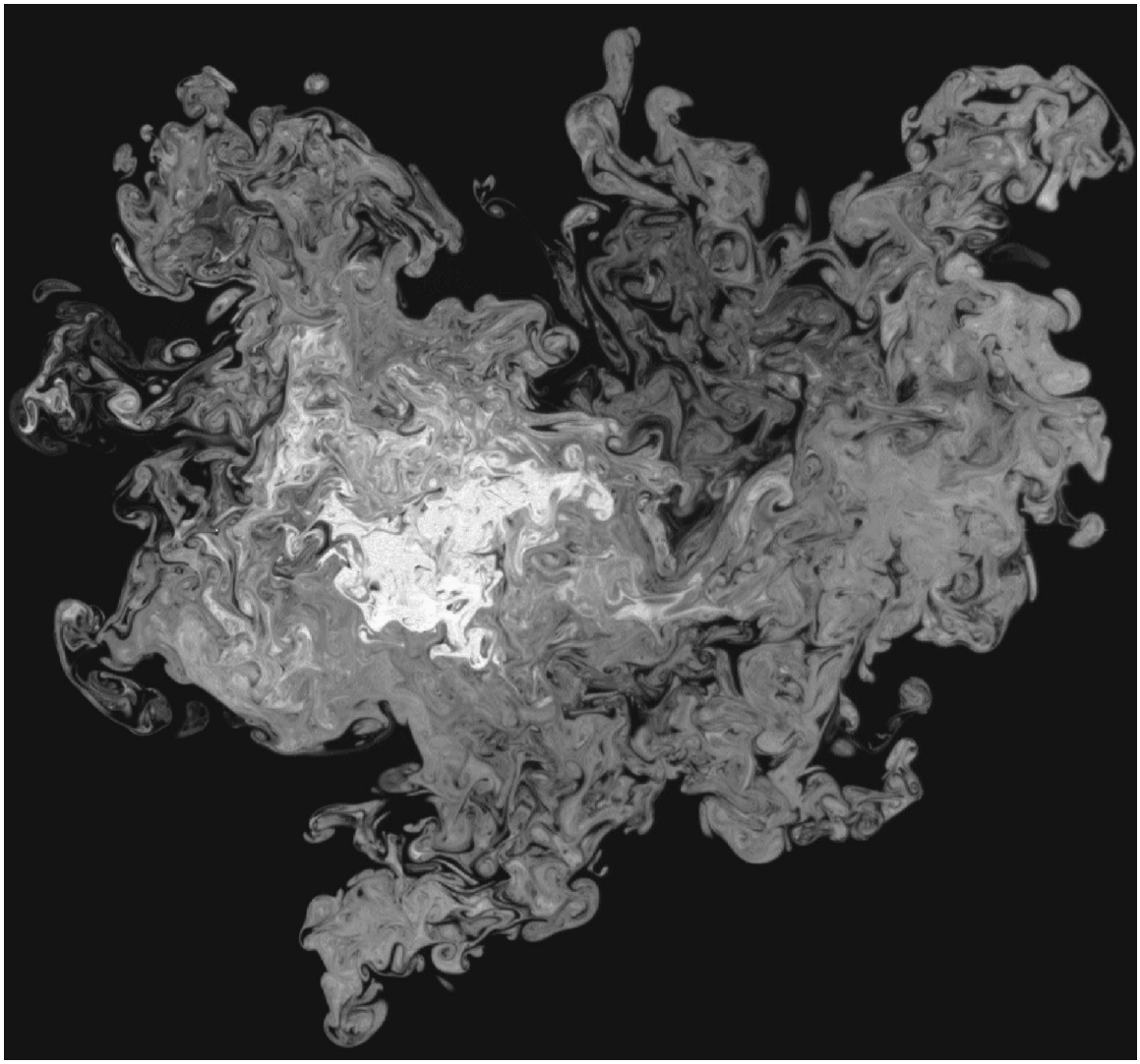

FIG. 10. Two-dimensional spatial slice of the concentration field in the similarity plane and far field of a liquid-phase turbulent jet recorded at $\mathrm{Re}\sim 10^4$ using laser-induced fluorescence and digital-imaging techniques. Grey levels, from black to white, denote increasing values of the jet-fluid concentration.

fluorescence and high-resolution digital-imaging techniques [29,45,46]. The jet Reynolds number, $\mathrm{Re}\simeq 9.0\times 10^3$, is near the regime of fully-developed turbulent flow. The Schmidt number of the scalar species, aqueous disodium fluorescein, is $\mathrm{Sc}\sim 10^3$. Gray levels, from black to white, denote increasing values of the jet-fluid concentration. Of particular interest in the context of quantifying mixing is the structure of mixed-fluid interfaces or level sets of concentration. Figure 11 depicts a scalar level set extracted from the two-dimensional image data of Fig. 10. The scalar threshold corresponds to the peak of the jet-fluid concentration PDF at this Re. The examination of scaling or fractal behavior of the fluid interfaces is facilitated in the present images because these measurements were conducted in the similarity plane and at a particular distance downstream ($z/d_0\simeq 275$) to avoid effects of the downstream variation of scales in this flow. The Péclet number, $\mathrm{Pe}=\mathrm{Re}\,\mathrm{Sc}\sim 10^7$, is relevant for an investigation of scaling properties of fluid interfaces which have been proposed in the high-Pe regime.

The two-dimensional scalar field was represented in terms of bilinear B-spline functions fitted through the normalized and calibrated digital-image data. The level sets were computed from the scalar field using the B-spline function representation evaluated at a sub-pixel resolution of $\lambda_p/4$. Coverage statistics of the 2D level sets were computed using a 2D box-counting algorithm in which a δ_b-sized bounding box was identified and partitioned into contiguous λ boxes, to compute the coverage fraction of the number of boxes that cover the level set, as a function of scale. Six images at a Reynolds number of $\mathrm{Re}\simeq 9.0\times 10^3$ were processed to compute ensemble-averaged coverage statistics. Linear, one-dimensional transects were also constructed that pass through the level sets. Examples are shown in Fig. 12 which depicts 1D transects through the two-dimensional level-set data of Fig. 11. The transects were generated via a Monte Carlo Poisson algorithm to produce random linear cuts that lie within the bounding box of the level set as indicated in Fig. 12. For the 1D coverage statistics, 10^3 transects were constructed for each level set and the level-crossing locations were box-counted, or tile-counted, using a 1D coverage procedure [47].

High- and low-dimensional transects of complex multidi-

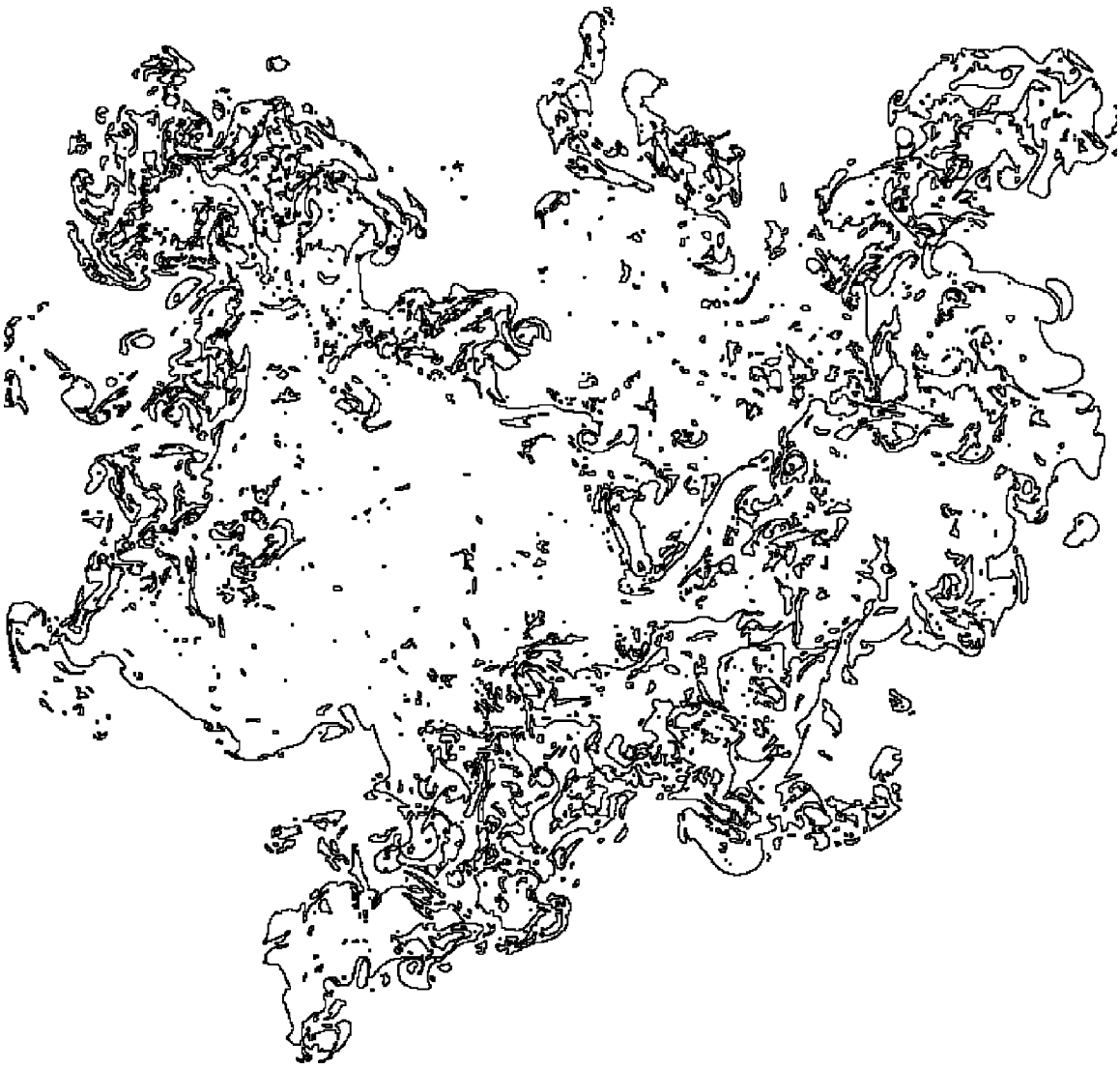

FIG. 11. Level set of the concentration field derived from the image data of Fig. 10. The scalar threshold corresponds to the peak of the jet-fluid concentration PDF at Re$\sim 10^4$.

mensional structures may be expected to have scale distributions that are similar, at least qualitatively. For surfaces in 3D space, for example, 2D planar transects consist of lines or curves with a scale distribution which may be similar to the full scale distribution; 1D linear transects consist of points whose statistics may be expected to reflect the higher-dimensional behavior. Figures 13 and 14 show the ensemble-averaged coverage fraction, $F_d(\lambda)$, coverage dimension, $D_d(\lambda)$, and LEB-scale PDF, $f_d(\lambda)$, for both the two-dimensional scalar level sets and the corresponding one-dimensional transects, derived from the jet measurements at Re$\simeq 9\times 10^3$. The smallest diffusion scale of the concentration field is estimated to be $\log_{10}(\lambda_{\mathcal{D}}/\delta_b)\simeq -3.0$, on the jet axis. The spatial scale, λ, is normalized by the size of the 2D-transect bounding box, δ_b. For both the 2D and 1D data, the coverage fraction tends to unity at large scales, as expected. At scales smaller than δ_b, however, the measurements show that

$$F_2(\lambda) > F_1(\lambda), \tag{40}$$

i.e., the higher-dimensionality transects exhibit a larger cov-

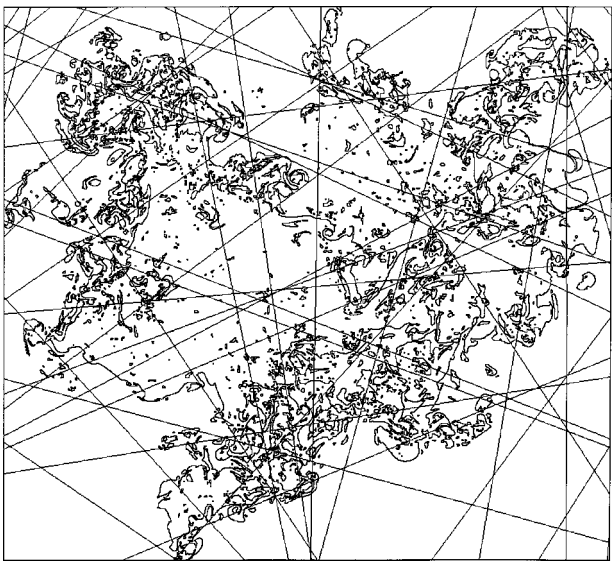

FIG. 12. One-dimensional spatial transects through the level set depicted in Fig. 11. The linear transects were generated by a Poisson process. The bounding box is also indicated.

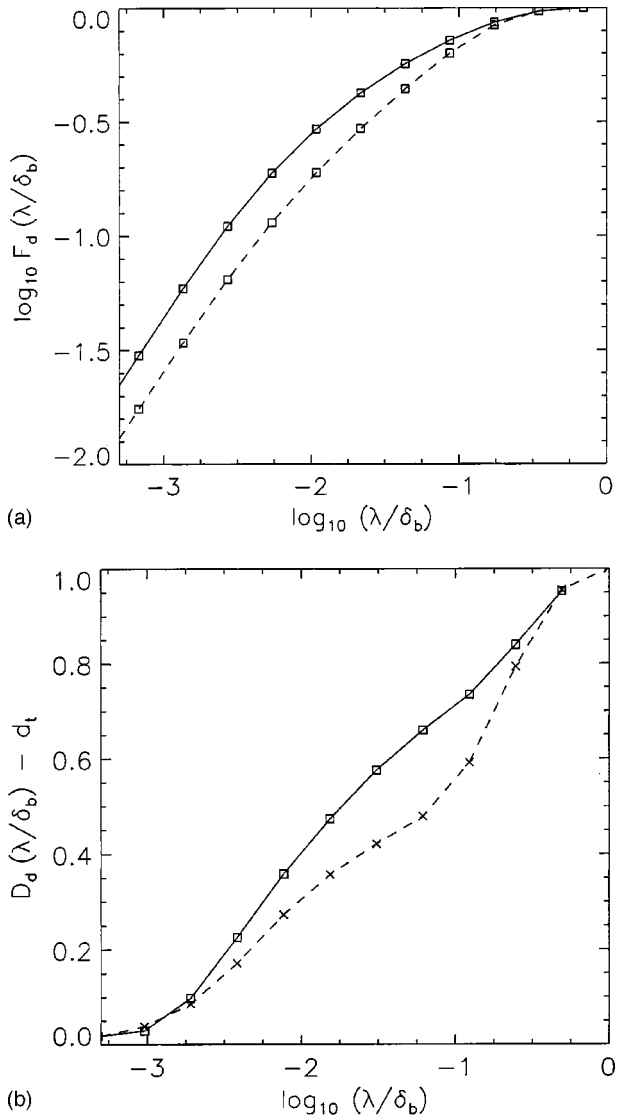

FIG. 13. Scale dependence of coverage fraction (a) and relative coverage dimension (b) of spatial two-dimensional (solid line) and one-dimensional (dashed line) jet transects.

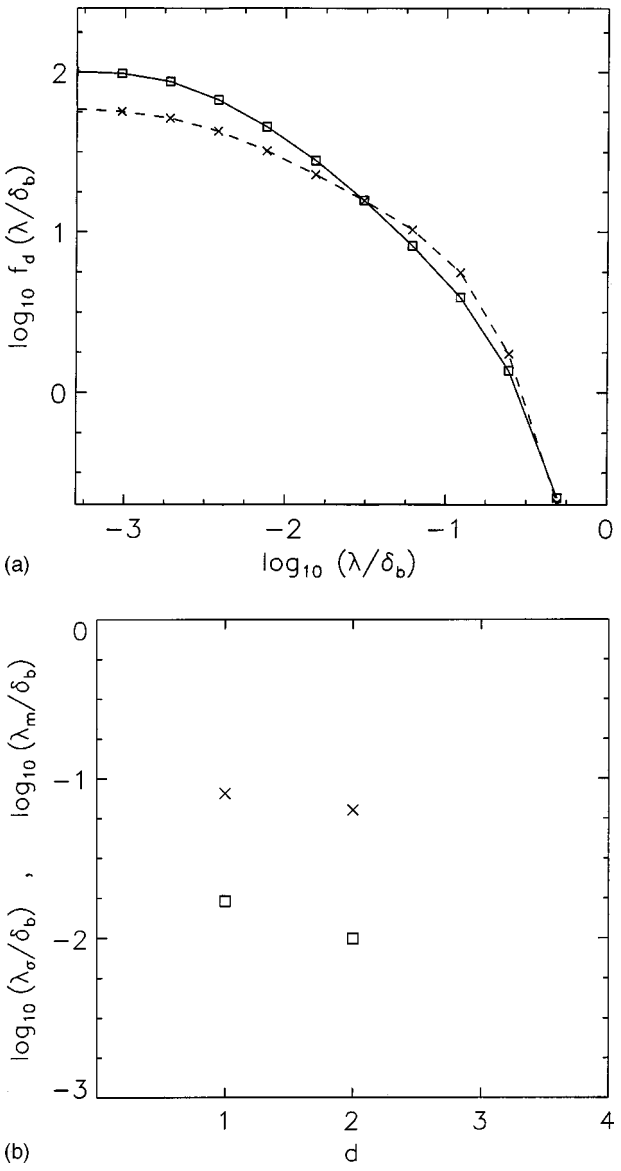

FIG. 14. (a) LEB-scale PDF for two-dimensional (solid line) and one-dimensional (dashed line) transects. (b) Dependence of the mean LEB scale (crosses) and the normalized inverse-area-volume-ratio scale (squares) on the transect dimension.

erage fraction. The coverage fraction is the geometric probability that a randomly-placed box contains a part of the object and this will be, in general, larger for the higher-dimensional transects. The coverage dimension for the jet transects is shown in Fig. 13(b) and is plotted as the relative coverage dimension, $D_d(\lambda)-d_t$, where d_t is the topological dimension. For the 2D as well as 1D level sets, the coverage dimension increases smoothly with scale, λ. This quantity ranges from zero, at the small scales, to unity, at the large scales,

$$0 \leqslant D_d(\lambda)-d_t \leqslant 1, \tag{41}$$

for the fluid-interface data. The lower limit will be 0 regardless of the topological dimension, d_t, or embedding dimension, d. The upper limit will be 1 for points in 1D, curves in 2D, surfaces in 3D, etc. Such objects can be expected to arise in the study of mixed-fluid interfaces in turbulent flows. Higher upper limits of the relative coverage dimension are possible for curves embedded in 3D space, e.g., vortex lines.

The relative coverage dimensions, for the 1D and 2D data, agree at the smallest and largest scales, as expected. At intermediate scales, however, the measurements show that

$$D_2(\lambda)-1 > D_1(\lambda), \tag{42}$$

i.e., the higher-dimensionality transects, in this case, are found to be associated with a larger relative coverage dimension [47]. For objects that exhibit self-similar fractal scaling, an assumption is typically made that dimensions derived from transects should satisfy $D_{d+1}=D_d+1$. This assumption is related to a theorem which applies to Hausdorff dimensions of nearly all transects through a fractal object [48], where ''nearly all'' means except for a set of transects of probability measure zero. The present data correspond to a finite Reynolds number and the level sets cannot be considered as fractal, constant-dimension objects, which is one of the assumptions of this theorem. Also, the coverage dimen-

sions computed for the jet data are not Hausdorff dimensions but capacity, or Kolmogorov, dimensions for which there is no equivalent theorem. Nevertheless, the present conclusion that higher-dimensional box analysis captures more structure than ensemble-averaged lower-dimensional box analysis is qualitatively consistent with the behavior of spiral structures [15] and is in agreement with other spatial and temporal 1D measurements of interfaces in jets [43]. This behavior can be expected for fluid interfaces in other turbulent flows [36].

The coverage statistics of the present 1D transects are in agreement with the LEB-scale PDF for the present measurements is shown in Fig. 14(a). The data indicate that the probability density of a LEB scale increases continuously with decreasing scale, tending to a constant as $\lambda \to 0$. While the jet is not statistically homogeneous spatially, $f_d(\lambda)$ retains its meaning. For example, for the two-dimensional level sets, $f_2(\lambda)$ it is the PDF of the size of LEBs, randomly placed, interior to the δ_b-box. The data indicate that, $f_2(\lambda \to 0) > f_1(\lambda \to 0)$, i.e., the higher-dimensional transects are associated with a higher area-volume ratio, as anticipated [26]. The present data indicate that

$$f_2(\lambda) > f_1(\lambda) \quad \text{for } \lambda < \tilde{\lambda}, \tag{43}$$

while

$$f_2(\lambda) < f_1(\lambda) \quad \text{for } \lambda > \tilde{\lambda}, \tag{44}$$

where $\tilde{\lambda}$ appears as a crossover scale. In other words, above this scale, it is harder to find large-scale empty space, or regions not visited by the interface, for the 2D transects. Below the crossover scale, it is easier to find small-scale empty regions for the 2D transects. The apparent crossover scale in the LEB-scale PDF behavior is partly a consequence of the fact that the LEB-scale PDF is normalized. The mean LEB scale is larger for the lower-dimensional 1D transects, as shown in Fig. 14(b). The inverse area-volume scale measure is also larger in 1D, indicating a lower area-volume estimate, as expected [49]. Since the LEB-scale PDF is a scale-dependent area-volume measure, the data show that 1D-transect estimates of the area-volume ratio are underestimates at smaller scales and overestimates at larger scales, when compared to 2D transect measures. The jet-transect behavior is similar, in some respects, to Poisson-plane transects. A notable difference is that the mean LEB scale is identical to the inverse area-volume ratio scale, for the Poisson model, while $\lambda_m/\lambda_\sigma \sim 10$ for these jet data, cf. Fig. 4. Data from transects of different dimensionality can be compared in terms of the inverse of the point density in 1D, perimeter-area ratio in 2D, and area-volume ratio in 3D, such as the scale λ_σ. These considerations are especially important in the context of phenomena for which 3D measurements are not readily possible, e.g., rock-fracture or earthquake-fault networks.

In turbulent flows, in general, the scale-dependence of the coverage dimension and the corresponding LEB-scale PDF can be expected to reflect both the large-scale organized structure of the particular flow and generic small-scale characteristics. For example, in the coverage-dimension and scale-distribution behavior of the jet, exhibited in Figs. 13 and 14, respectively, a signature of the three-dimensional large structure of the jet can be discerned. At the small scales, the observed behavior can be modeled in terms of a lognormal distribution of scales,

$$f_2(\lambda) \propto \mathrm{erfc}[\{\ln(\lambda/l_m)/\sigma + \sigma/2\}/\sqrt{2}]/2l_m, \tag{45}$$

with $\log_{10}(l_m/\delta_b) \simeq -1.5$ and $\sigma \simeq 1.2$, as fitted to the inner scales [45]. Lognormal spacing-scale statistics have been reported at Reynolds numbers as high as $\mathrm{Re}_\lambda \sim 5000$ in plumes dispersing in the atmospheric surface layer [41]. Such statistics may be anticipated in various fragmentation/growth processes describable in terms of stochastic multiplicative sequences [50], and appear to be good candidates for quantifying the geometry of the Richardson-Kolmogorov cascade in turbulence, including both the break-up and pairing of vortical structures.

A significant question, fundamentally and practically, is whether fluid interfaces become more folded, more wrinkled, or both, as the Reynolds number is increased. Previous work has indicated that the concentration field in high-Reynolds-number incompressible shear flows becomes nearly homogeneous, corresponding to well-mixed fluid, where a large vortical structure is present [32,51,44,33,35]. One may expect, therefore, that the relative degree of folding of the interfaces may decrease with increasing Reynolds number reflecting the presence of the large structure. Curvature statistics of fluid interfaces [52–55] may be useful in this context to quantify the distribution of folds and wrinkles. In the present work, the scale-distributions framework leads naturally to two quantitative measures of folding and wrinkling of the interfaces. Based on the LEB scale distribution, $f(\lambda)$, and its physical meaning as the PDF of the size of the largest flow region not containing a part of the interface, let us define a dimensionless measure of folding as

$$\mathcal{F} = \left(\int_{\lambda^*}^{\delta} f(\lambda) d\lambda \right)^{-1}, \tag{46}$$

and a dimensionless measure of wrinkling as

$$\mathcal{W} = \int_{f^*}^{f_0} \lambda \, df(\lambda), \tag{47}$$

where $f^* = f(\lambda^*)$, $f_0 = \lim_{\lambda \to 0} f(\lambda) = 1/\lambda_m$. The scale, λ^*, is a reference scale such that interfacial features of size $\lambda > \lambda^*$ may be considered as folds, and features of size $\lambda < \lambda^*$ may be considered as wrinkles. In turbulent shear flows, the interfacial folds can be viewed as features that are directly related to and generated by the large-scale vortical structures [56]. The interfacial wrinkles may be viewed as the result of Richardson-Kolmogorov cascades to higher wave numbers, i.e., large eddies breaking up into smaller eddies, or because of internal small-scale instabilities of the large structures and associated three-dimensional vortex stretching [56]. Figure 15 is a schematic of four scenaria of fluid interfaces with varying degrees of folding and wrinkling. Scenario (b) shows a schematic of an interface with low folding number but high wrinkling number, which can be expected to be relevant for high-Reynolds-number mixing in incompressible flows, because of the presence of large vortical structures. Mixing in compressible flows, in which it is found that vortical motions are not as dynamically impor-

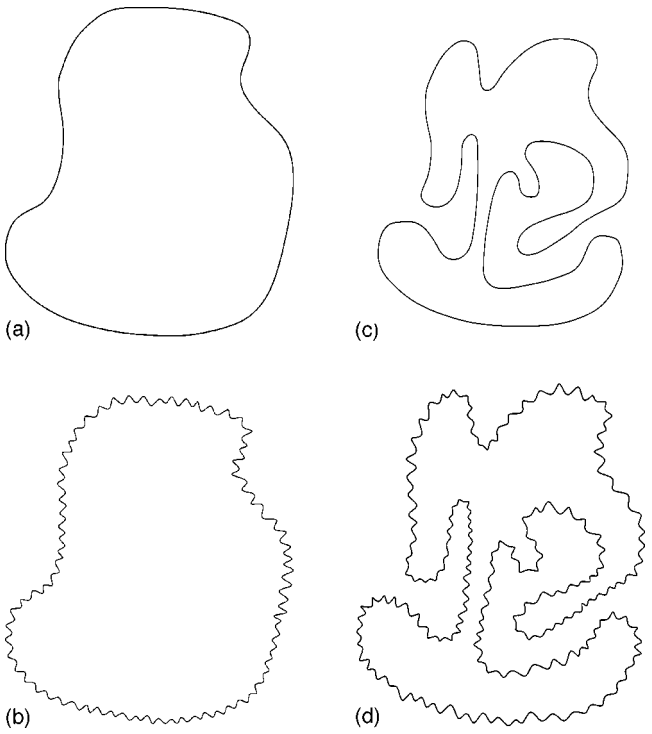

FIG. 15. Schematic of fluid interfaces with varying degrees of folding and wrinkling, which can be quantified by a folding number, $\mathcal{F}$, and a wrinkling number, $\mathcal{W}$. (a) Low $\mathcal{F}$ and low $\mathcal{W}$. (b) Low $\mathcal{F}$ and high $\mathcal{W}$. (c) High $\mathcal{F}$ and low $\mathcal{W}$. (d) High $\mathcal{F}$ and high $\mathcal{W}$. Scenario (b) may be expected to be relevant for high-Reynolds-number mixing in incompressible flows, in those flow regions where large vortical structures are present. Scenario (d) would be more relevant for compressible turbulent mixing.

tant for mixing as in the incompressible case, may be expected to be characterized more accurately by scenario (d) which shows a schematic of an interface with high folding number and high wrinkling number. For the reference scale, λ^*, a good choice would be the Liepmann scale, λ_L, which is the smallest scale that can be generated directly from the outer δ-size scale of the flow, e.g., $\lambda_L/\delta \sim \mathrm{Re}^{-1/2}$ for the laminar boundary-layer thickness that can be generated by a single δ-sized sweep across the turbulent region [7]. This scale is not expected to depend on the Schmidt number since large-scale vortical structure is independent of scalar diffusivity. The Liepmann scale is closely related to the Taylor scale, in terms of the Reynolds-number dependence, and marks the separation between the range of scales that are generated directly from outer scales of the flow and the range of scales that correspond to outer-scale-independent dynamics.

IV. CONCLUSIONS

The proposed framework can be used to quantify the distribution of scales spanned by complex surfaces such as fluid interfaces in turbulent flows. The framework involves a multidimensional measure of scale and, therefore, can be used to quantify the four-dimensional space-time evolution of fluid interfaces. Other level sets, such as vorticity- or velocity-magnitude isosurfaces, can also be analyzed and modeled with this framework. The proposed measure of scale distributions can also be used to identify the geometric-scale analogs of classical turbulence scales such as the Kolmogorov, Taylor, or Batchelor scales. The inverse of the area-volume ratio of the level sets can be computed, or modeled, as the inverse of the small-scale limit of the LEB-scale PDF, and is important to quantify the mixing efficiency in the case of mixed-fluid interfaces. Such scales are useful in analyzing and comparing Reynolds-number and Schmidt-number effects on mixing in different turbulent flows.

The dimensionless folding and wrinkling numbers are expected to be useful for quantifying the contributions of the large-scale and small-scale turbulent flow structure to the interfacial geometry. These folding and wrinkling measures can be used to compare quantitatively interfaces generated by turbulent flows, to quantify Reynolds number and Schmidt number effects, to assess the performance of proposed flow-control techniques on mixing enhancement or reduction, and to quantify the contributions of the large- and small-scale interfacial geometry to laser beam propagation, wandering, and attenuation in optically-active gases, for example. Also, these measures can be expected to be helpful to quantify the relative degree of organization of the large structure in a particular realization of the flow and to evaluate the extent to which flow-control schemes can be used to organize the large structure of the turbulence and thus to enable an efficient study of the properties of the large structures.

ACKNOWLEDGMENTS

This research is part of a larger effort to investigate turbulent flows and mixing, and is supported by the National Science Foundation and the U.S. Air Force Office of Scientific Research. Useful discussions with C. L. Bond, M. C. Cross, J. C. Catrakis, P. E. Dimotakis, M. Gharib, J. W. Hearn, H. G. Hornung, J. C. R. Hunt, A. Leonard, H. W. Liepmann, M. G. Mungal, D. I. Pullin, A. Roshko, P. G. Saffman, E. Titi, and E. Villermaux are gratefully acknowledged.

[1] G.I. Taylor, Proc. R. Soc. London, Ser. A **151**, 421 (1935).
[2] G.I. Taylor, Proc. R. Soc. London, Ser. A **164**, 476 (1938).
[3] T. von Kármán and L. Howarth, Proc. R. Soc. London, Ser. A **164**, 192 (1938).
[4] T. von Kármán and L. Howarth, J. Mar. Res. **7**, 252 (1948).
[5] A.N. Kolmogorov, Dokl. Akad. Nauk SSSR **30**, 301 (1941).
[6] K.R. Sreenivasan, Annu. Rev. Fluid. Mech. **23**, 539 (1991).
[7] P. E. Dimotakis, J. Fluid Mech. **409**, 69 (2000); P. E. Dimotakis and H. J. Catrakis, in *Mixing: Chaos and Turbulence*, edited by H. Chaté and E. Villermaux (Plenum, New York, 1999), pp. 59–144.
[8] B.B. Mandelbrot, J. Fluid Mech. **72**, 401 (1975).
[9] K.R. Sreenivasan and C. Meneveau, J. Fluid Mech. **173**, 357 (1986).

[10] P. Constantin, I. Procaccia, and K.R. Sreenivasan, Phys. Rev. Lett. **67**, 1739 (1991).
[11] E. Villermaux and C. Innocenti, J. Fluid Mech. **393**, 123 (1999).
[12] L.P. Kadanoff, Phys. Today **40**, 7 (1987).
[13] M.C. Cross and P.C. Hohenberg, Rev. Mod. Phys. **65**, 851 (1993).
[14] B.B. Mandelbrot, *The Fractal Geometry of Nature* (Freeman, New York, 1983).
[15] J.C. Vassilicos and J.C.R. Hunt, Proc. R. Soc. London, Ser. A **435**, 505 (1991).
[16] A.S. Michailov and A.Y. Loskutov, *Foundations of Synergetics II: Complex Patterns* (Springer, New York, 1991).
[17] G. Galilei, *Discorsi e Dimostrazioni Matematiche Intorno a' Due Nuove Science, Leiden, 1638*, translated by S. Drake (University of Wisconsin Press, 1974).
[18] L.F. Richardson, General Systems Yearbook **6**, 139 (1961).
[19] H. Takayasu, J. Phys. Soc. Jpn. **51**, 3057 (1982).
[20] S. Matsuura, S. Tsurumi, and N. Imai, J. Chem. Phys. **84**, 539 (1986).
[21] M. Suzuki, Prog. Theor. Phys. **71**, 1397 (1984).
[22] D.M. Mark and P.B. Aronson, J. Int. Assoc. Math. Geol. **16**, 671 (1984).
[23] J.P. Chiles, Math. Geol. **20**, 631 (1988).
[24] J.P. Rigaut, in *Fractals: Non-Integral Dimensions and Applications*, edited by G. Cherbit (Wiley, New York, 1991), pp. 151–187.
[25] P.N. Brandt, R. Greimel, E. Guenther, and W. Mattig, in *Applying Fractals in Astronomy*, edited by A. Heck and J. M. Perdang (Springer, Berlin), pp. 77–96.
[26] C. Castagnoli and A. Provenzale, Astron. Astrophys. **246**, 634 (1991).
[27] R.E. Amritkar, Indian J. Pure Appl. Phys. **32**, 595 (1994).
[28] H. J. Catrakis, PhD. thesis, California Institute of Technology, 1996.
[29] H.J. Catrakis and P.E. Dimotakis, J. Fluid Mech. **317**, 369 (1996).
[30] D.I. Pullin and P.G. Saffman, Annu. Rev. Fluid Mech. **30**, 31 (1998).
[31] P.E. Dimotakis and G.L. Brown, J. Fluid Mech. **78**, 535 (1976).
[32] J. Konrad, Ph.D. thesis, California Institute of Technology, 1976.
[33] A. Roshko, in *The Global Geometry of Turbulence*, edited by J. Jiménez (Plenum, New York, 1991), pp. 3–11.
[34] H.J. Catrakis, J. Fluid Mech (to be published).
[35] P.E. Dimotakis, H.J. Catrakis, and D.C.L. Fourguette, J. Fluid Mech. (to be published).
[36] P.E. Dimotakis, Nonlin. Sci. Today, **1**, 1 (1991); **1,** 27 (1991).
[37] M.S. Longuet-Higgins, Proc. R. Soc. London, Ser. A **246**, 98 (1958).
[38] A. Papoulis, *Probability, Random Variables, and Stochastic Processes*, 3rd ed. (McGraw-Hill, New York, 1991).
[39] H.C. Tuckwell, *Elementary Applications of Probability Theory*, 2nd ed. (Chapman & Hall, London, 1995).
[40] K.R. Sreenivasan, A. Prabhu, and R. Narasimha. J. Fluid Mech. **137**, 251 (1983).
[41] E. Yee, R. Chan, P.R. Kosteniuk, G.M. Chandler, C.A. Biltoft, and J.F. Bowers, Boundary-Layer Meteorol. **73**, 53 (1995).
[42] H.W. Liepmann, Helv. Phys. Acta **22**, 119 (1949).
[43] P.L. Miller and P.E. Dimotakis, Phys. Fluids A **3**, 168 (1991)
[44] P.E. Dimotakis, in *Turbulent Reactive Flow*, edited by R. Borghi and S.N.B. Murthy (Springer, Berlin, 1989), pp. 417–485.
[45] H.J. Catrakis and P.E. Dimotakis, Phys. Rev. Lett. **77**, 3795 (1996).
[46] H.J. Catrakis and P.E. Dimotakis, Phys. Rev. Lett. **80**, 968 (1998).
[47] H.J. Catrakis and C.L. Bond, Phys. Fluids (to be published).
[48] K.J. Falconer, *Geometry of Fractal Sets* (Cambridge University Press, Cambridge, England, 1985).
[49] S. Corrsin, Q. Appl. Math. **12**, 404 (1955).
[50] A.N. Kolmogorov, Dokl. Akad. Nauk SSSR **31**, 99 (1941).
[51] M.G. Mungal and P.E. Dimotakis, J. Fluid Mech. **148**, 349 (1984).
[52] S.B. Pope, Int. J. Eng. Sci. **26**, 445 (1988).
[53] S.B. Pope, P.K. Yeung, and S.S. Girimaji, Phys. Fluids A **1**, 2010 (1989).
[54] S.B. Girimaji and S.S. Pope, J. Fluid Mech. **220**, 427 (1990).
[55] B.J. Gluckman, H. Willaime, and J.P. Gollub, Phys. Fluids A **5**, 647 (1993).
[56] G.L. Brown and A. Roshko, J. Fluid Mech. **64**, 775 (1974).